

Multi-element Flux Analysis for the Incorporation of Detailed Kinetic Mechanisms in Reactive Simulations

Kaiyuan He, Ioannis P. Androulakis, and Marianthi G. Ierapetritou*

Department of Chemical and Biochemical Engineering, Rutgers, The State University of New Jersey, Piscataway, New Jersey 08854

Received July 28, 2009. Revised Manuscript Received November 3, 2009

A method is proposed in this paper based on element flux analysis, which is used for the efficient incorporation of detailed fuel combustion and pollutant formation mechanisms in realistic flow calculations. Specifically, a multi-element flux analysis and a tree searching procedure are introduced to incorporate NO_x and soot formation in reduced mechanisms that are generated on the fly during the simulation in addition to the main fuel oxidation network. The inclusion of detailed kinetics in the simulation facilitates the study of combustion characteristics, including ignition time delay, pollutant emission level, and species concentration history. A reaction mechanism of the aviation fuel JP-10 with NO_x and soot formation is used to demonstrate the proposed approach. Simulation results using the on-the-fly reduced representation are compared to experimental data, and excellent agreement was observed.

Introduction

Fossil fuels have contributed approximately 85% of the energy consumed in the United States each year, with transportation being an essential part. As future global energy and environment regulations become more stringent, the importance of research oriented on saving energy along with reducing pollutant emissions and greenhouse gases has continuously grown over the last few decades. In recent studies, detailed chemical kinetic mechanisms for realistic fuels have been developed to predict characteristics such as ignition delay, combustion efficiency, and pollutant formation.^{1–4} In addition to fuel oxidation mechanisms, NO_x , soot, and polycyclic aromatic

hydrocarbon (PAH) formation mechanisms are also developed to predict pollutant emissions in engine combustion.^{5–11}

Detailed kinetic mechanisms can provide a comprehensive description of fuel chemistry. However, they usually consist of hundreds of species and thousands of reactions. The incorporation of these detailed mechanisms in computational fluid dynamic (CFD) calculations is computationally expensive and often times prohibitive. Thus, two broad categories of approximation approaches have been proposed to integrate CFD and detailed chemical kinetics: (a) detailed flow calculation coupled with simplified kinetic models and (b) detailed kinetic mechanisms coupled with a simplified description of the flow field. Approximation approaches focusing on kinetic reduction encompass a multitude of techniques, including global lumping techniques, skeletal reduction, and adaptive reduction. Kuo and Wei¹² proposed an approach that lumps concentrations of chemical species into a reduced species set and lumps elementary reactions into a few global steps. Approaches aiming at developing skeletal kinetic mechanisms include sensitivity analysis,^{13,14} quasi-steady-state approximation (QSSA) or partial equilibrium approximation,^{15,16} and optimization-based approaches.^{17–19} Adaptive kinetic

*To whom correspondence should be addressed: 98 Brett Road, Piscataway, NJ 08854. Telephone: (732) 445-2971. Fax: (732) 445-2581. E-mail: marianth@soemail.rutgers.edu.

(1) Dagaut, P.; El Bakali, A.; Ristori, A. The combustion of kerosene: Experimental results and kinetic modelling using 1-to 3-component surrogate model fuels. *Fuel* **2006**, *85* (7–8), 944–956.

(2) Li, S. C.; Varatharajan, B.; Williams, F. A. Chemistry of JP-10 ignition. *AIAA J.* **2001**, *39* (12), 2351–2356.

(3) Lindstedt, R. P.; Maurice, L. Q. Detailed chemical-kinetic model for aviation fuels. *J. Propul. Power* **2000**, *16* (2), 187–195.

(4) Schulz, W. D. Oxidation products of a surrogate JP-8 fuel. *Prepr.–Am. Chem. Soc., Div. Pet. Chem.* **1991**, *37* (2), 383–392.

(5) GRI-Mech 3.0 (<http://www.me.berkeley.edu/gri-mech/>).

(6) Glaude, P. A.; Pitz, W. J.; Thomson, M. J. Chemical kinetic modeling of dimethyl carbonate in an opposed-flow diffusion flame. *Proc. Combust. Inst.* **2005**, *30*, 1111–1118.

(7) Li, S. C.; Williams, F. A. NO_x formation in two-stage methane–air flames. *Combust. Flame* **1999**, *118* (3), 399–414.

(8) Richter, H.; Granata, S.; Green, W. H.; Howard, J. B. Detailed modeling of PAH and soot formation in a laminar premixed benzene/oxygen/argon low-pressure flame. *Proc. Combust. Inst.* **2005**, *30*, 1397–1405.

(9) Riesmeir, E.; Honnet, S.; Peters, N. Flamelet modeling of pollutant formation in a gas turbine combustion chamber using detailed chemistry for a kerosene model fuel. *J. Eng. Gas Turbines Power* **2004**, *126*, 899–905.

(10) Warnatz, J.; Klaus, P. CEC reaction mechanism for methane/air combustion (<http://www.ca.sandia.gov/tdf/3rdworkshop/chemmech/>).

(11) Wen, Z.; Yun, S.; Thomson, M. J.; Lightstone, M. F. Modeling soot formation in turbulent kerosene/air jet diffusion flames. *Combust. Flame* **2003**, *135* (3), 323–340.

(12) Wei, J.; Kuo, J. A lumping analysis in monomolecular reaction systems. Analysis of exactly lumpable systems. *Ind. Eng. Chem. Fundam.* **1969**, *8* (1), 114–123.

(13) Rabitz, H.; Kramer, M.; Dacol, D. Sensitivity analysis in chemical kinetics. *Annu. Rev. Phys. Chem.* **1983**, *34*, 419–461.

(14) Turanyi, T. Reduction of large reaction mechanisms. *New J. Chem.* **1990**, *14*, 795–803.

(15) Chen, J. Y. A general procedure for constructing reduced reaction mechanisms with given independent reactions. *Combust. Sci. Tech.* **1988**, *57*, 89–94.

(16) Peters, N. Systematic reduction of flame kinetics—Principles and details. Proceedings of the 11th International Colloquium on Dynamics of Explosions and Reactive Systems, Warsaw, Poland, 1988; pp 67–86.

(17) Androulakis, I. P. Kinetic mechanism reduction based on an integer programming approach. *AIChE J.* **2000**, *46* (2), 361–371.

(18) Bhattacharjee, B.; Schwer, D. A.; Barton, P. I.; Green, W. H. Optimally reduced kinetic models: Reaction elimination in large-scale kinetic mechanisms. *Combust. Flame* **2003**, *135* (3), 191–208.

(19) Petzold, L.; Zhu, W. J. Model reduction for chemical kinetics: An optimization approach. *AIChE J.* **1999**, *45* (4), 869–886.

reduction strategies have been explored to use different, reduced, mechanisms for different conditions. Several adaptive schemes have been proposed, including *in situ* adaptive tabulations (ISATs),²⁰ “store and retrieve” representations,²¹ mathematical programming approaches,²² and graph-based reduction approaches.²³ In the engine simulation community, a number of approaches have centered on simplified flow calculations. This is usually achieved using the so-called “zone” approach. The earliest and simplest example of this type of model was single-zone models,²⁴ which considered the entire engine reactor to be a single cell. Later, multi-zone models have been developed that divide the combustion chamber into multiple zones based on physical conditions.²⁵

We have previously introduced an on-the-fly kinetic reduction method based on element flux analysis to take advantage of both accurate CFD models and detailed kinetic mechanisms.²⁶ Element flux analysis provides an indicator to quantify species activity, which can be implemented in mechanism reduction to identify redundant species and reactions. The on-the-fly scheme enables efficient integration of detailed fuel kinetics with CFD calculation, which is especially useful in the simulation of complex fuel combustion systems. Because the combustion process studied in our previous work mainly involved hydrocarbon oxidation, only carbon element flux was incorporated to capture carbon transformations. However, when the flux analysis method is to be extended to systems that involve NO_x formation, it becomes necessary to incorporate multi-element analysis in the reduction scheme to capture different reaction networks in the system. Another drawback of the reduction scheme employed in ref 26 is that soot formation cannot be well-captured during the reduction procedure. This is due to the fact that soot species usually have much smaller flux compared to the fuel oxidation network. Therefore, when the element flux pointers are sorted to identify key species, soot species are always below the cutoff and excluded from the reduced mechanisms. Moreover, although nitrogen flux can uniquely capture the NO_x formation network, there is no unique element for the soot formation network.

To address the aforementioned limitations of the reduction scheme, an efficient multi-element (C, H, O, and N) flux analysis framework combined with a tree searching procedure are introduced in this work to incorporate NO_x and soot formation in the reduced mechanisms. The proposed method is demonstrated using a JP-10 mechanism² with NO_x and soot formation.⁸ JP-10 is a single-component hydrocarbon

(C₁₀H₁₆) aviation turbine fuel, which is used in volume-limited combustion chambers, such as those of supersonic-combustion ramjets and pulse-detonation engines. The high energy density and the very low freezing point of the fluid have made JP-10 the only air-breathing missile fuel used by the United States at the present time.²⁷ Unlike other practical fuels, JP-10, being a pure component, is amenable to theoretical modeling. The JP-10 decomposition and combustion mechanism used in this work was proposed by Li et al.,² which employed a number of approximations in the decomposition of JP-10 to species of smaller size. Despite its brevity in JP-10 decomposition, the mechanism is capable of accurately predicting the ignition delay times^{2,28} and the combustion of smaller molecules formed in JP-10 decomposition.^{28,29}

In this work, the JP-10 mechanism is employed to demonstrate the proposed multi-element flux analysis method as well as to perform, for the first time, the simulation of JP-10 combustion in CFD with detailed chemistry. The remaining paper is organized as follows. First, the mechanism reduction framework including NO_x and soot formation is presented. Then, the methodology is employed to study JP-10 oxidation with soot and NO_x formation. Discussions and conclusions are finally provided.

Mechanism Reduction Based on Element Flux Analysis

The on-the-fly reduction scheme reduces the detailed mechanism based on element flux analysis. In our previous work,¹⁷ we demonstrated how the concept of element flux analysis, first introduced by Revel et al.,³⁰ provides a pointer to quantify the activity of species in a reaction system. The instantaneous elemental flux of atom *A* from species *j* to species *k* through reaction *i*, denoted as \dot{A}_{ijk} , is defined in eq 1. The total instantaneous flux between species *j* and *k* can be calculated by summing \dot{A}_{ijk} over all of the reactions in which species *j* and *k* are involved, as represented in eq 2

$$\dot{A}_{ijk}(t) = q_i(t) \frac{n_{A,j} n_{A,k}}{N_{A,i}} \quad (1)$$

$$\bar{\dot{A}}_{jk}(t) = \sum_{i=1}^{N_R} \dot{A}_{ijk}(t) \quad (2)$$

where $q_i(t)$ is the instantaneous rate of reaction *i* (mol/s), $n_{A,j}$ is the number of atoms *A* in species *j*, $n_{A,k}$ is the number of atoms *A* in species *k*, $N_{A,i}$ is the total number of atoms *A* in reaction *i*, and N_R represents the number of reactions that these species participate in as reactants or products. However, we recently demonstrated²³ that eqs 1 and 2 do not properly represent element flux for quasi-steady-state species induced by partial equilibrium reactions. This is due to the small net reaction rates of partial equilibrium reactions compared to their respective forward and reverse reaction rates. Therefore, the flux pointer \dot{A}_{ijk} calculated through eq 1 is small, although a very fast element transition is taking place between species *j* and *k* through reaction *i*. To avoid underestimation of element flux for these quasi-steady-state species,

(20) Pope, S. B. Computationally efficient implementation of combustion chemistry using *in situ* adaptive tabulation. *Combust. Theory Modell.* **1997**, *1* (1), 41–63.

(21) Androulakis, I. P. “Store and retrieve” representations of dynamic systems motivated by studies in gas phase chemical kinetics. *Comput. Chem. Eng.* **2004**, *28* (11), 2141–2155.

(22) Banerjee, I.; Ierapetritou, M. G. Development of an adaptive chemistry model considering micromixing effects. *Chem. Eng. Sci.* **2003**, *58* (20), 4537–4555.

(23) He, K.; Ierapetritou, M. G.; Androulakis, I. P. A graph-based approach to developing adaptive representations of complex reaction mechanisms. *Combust. Flame* **2008**, *155* (4), 585–604.

(24) Najt, P. M.; Forster, D. E. Compression-ignited homogeneous charge combustion. SAE Tech. Pap. 830264, 1983.

(25) Babajimopoulos, A.; Assanis, D. N.; Flowers, D. L.; Aceves, S. M.; Hessel, R. P. A fully integrated CFD and multi-zone model with detailed chemical kinetics for the simulation of PCCI engines. Proceedings of the 15th International Multidimensional Engine Modeling Users’ Group Meeting, Detroit, MI, 2005.

(26) He, K.; Androulakis, I. P.; Ierapetritou, M. G. On-the-fly reduction of kinetic mechanisms using element flux analysis. *Chem. Eng. Sci.* **2009**, DOI: 10.1016/j.ces.2009.09.073.

(27) Bruno, T. J.; Huber, M. L.; Laesecke, A.; Lemmon, E. W.; Perkins, R. A. Thermochemical and thermophysical properties of JP-10, NISTIR 6640, National Institute of Standards and Technology, Boulder, CO, 2006.

(28) Nakra, S.; Green, R. J.; Anderson, S. L. Thermal decomposition of JP-10 studied by micro-flowtube pyrolysis–mass spectrometry. *Combust. Flame* **2006**, *144* (4), 662–674.

(29) Petrova, M. V.; Williams, F. A. A small detailed chemical-kinetic mechanism for hydrocarbon combustion. *Combust. Flame* **2006**, *144* (3), 526–544.

(30) Revel, J.; Boettner, J. C.; Cathonnet, M.; Bachman, J. S. Derivation of a global chemical kinetic mechanism for methane ignition and combustion. *J. Chim. Phys. Phys. Chim. Biol.* **1994**, *91* (4), 365–382.

Table 1. Element Flux of Stoichiometric JP-10/Air Combustion with NO_x Formation^a

		C			O			H			N		
T = 805 K	JP-10	C ₅ H ₈	1401.3	O ₂	HO ₂	1057.1	JP-10	C ₅ H ₈	2150.4	N ₂	N ₂ O	0.0159	
		C ₃ H ₅	C ₃ H ₆	655.6	OH	H ₂ O	294.2	C ₃ H ₅	C ₃ H ₆	1078.6	N ₂	N	0.0001
		JP-10	C ₃ H ₅	514.3	O ₂	O	214.9	JP-10	C ₃ H ₅	821.6	N ₂	HCN	0.0001
		C ₅ H ₈	C ₃ H ₄	423.3	CH ₂ CHO	CH ₂ CO	187.0	C ₅ H ₈	C ₃ H ₅	688.3	N	NO	0.0001
		C ₅ H ₈	C ₃ H ₅	423.3	HO ₂	H ₂ O ₂	181.6	C ₅ H ₈	C ₃ H ₄	550.7	N ₂	N ₂ H	0.0000
		JP-10	C ₂ H ₄	373.9	O ₂	CH ₂ CHO	179.0	C ₂ H ₃	CH ₂ CHO	537.1	NO	NO ₂	0.0000
		JP-10	C ₂ H ₂	364.2	HO ₂	OH	167.5	JP-10	C ₂ H ₄	503.4	N ₂ H	N ₂ O	0.0000
		C ₂ H ₃	CH ₂ CHO	358.1	O ₂	CO	138.4	C ₅ H ₈	C ₂ H ₃	413.0	N ₂ O	NO	0.0000
		JP-10	C ₃ H ₃	326.5	O ₂	OH	120.1	JP-10	H	250.2	N ₂ O	NH	0.0000
		C ₅ H ₈	C ₂ H ₂	284.3	O	OH	96.6	C ₅ H ₈	HO ₂	221.0	NO	HNCO	0.0000
T = 1500 K	HCO	CO	897.6	O ₂	OH	1049.6	H	OH	1366.8	N ₂	N ₂ O	0.1743	
		CH ₂ O	HCO	746.9	O ₂	HO ₂	927.0	CH ₂ CO	CH ₃	1053.6	N ₂	N	0.0450
		C ₂ H ₄	C ₂ H ₃	722.3	O ₂	O	871.1	H	CH ₃	934.7	N ₂	HCN	0.0449
		CH ₂ CO	CO	704.0	OH	H ₂ O	864.1	C ₂ H ₄	C ₂ H ₃	868.1	N	NO	0.0369
		C ₂ H ₂	HCCO	622.7	O ₂	CO	699.4	OH	H ₂ O	822.8	N ₂	N ₂ H	0.0040
		CH ₂ CHO	CH ₂ CO	570.8	HCO	CO	566.4	H	H ₂	768.6	NO ₂	NO	0.0037
		HCCO	CO	548.8	CH ₂ CO	CO	498.8	C ₂ H ₃	CH ₂ CHO	716.9	N ₂ O	NO	0.0028
		CH ₂ CO	CH ₃	526.8	CH ₂ O	HCO	475.6	HCO	H	660.6	N ₂ O	NH	0.0025
		C ₂ H ₂	CH ₂ CO	521.9	HO ₂	OH	459.4	CH ₃	CH ₂ O	601.3	NO	HNCO	0.0012
		C ₂ H ₃	CH ₂ CHO	477.9	O ₂	CO ₂	279.1	CH ₂ CHO	CH ₂ CO	570.8	NH	HNO	0.0012
T = 2200 K	CO	CO ₂	21.3	OH	H ₂ O	27.0	OH	H	47.3	N ₂	NO	2.2828	
		HCO	0.2	CO	CO ₂	21.2	OH	H ₂ O	36.8	N ₂	N	2.2696	
		HCO	CO ₂	0.0	OH	CO ₂	20.9	OH	HO ₂	16.7	N	NO	2.2317
		CO	NCO	0.0	OH	HO ₂	20.4	H	H ₂ O	15.7	N ₂	N ₂ H	0.2782
		C ₂ H ₄ O	CO	0.0	O ₂	OH	19.5	H ₂	H	9.0	HNO	NO	0.2519
		C ₂ H ₄ O	CH ₃	0.0	O ₂	O	18.4	HO ₂	H ₂ O	5.6	NO	NO ₂	0.0870
		CH ₂ O	HCO	0.0	O	OH	15.4	H ₂	OH	4.5	NH	NO	0.0568
		CH ₃	CH ₂ O	0.0	HO ₂	O ₂	12.7	H ₂	H ₂ O	4.3	N ₂ H	N ₂ O	0.0564
		C ₂ H ₄ O	C ₂ H ₄	0.0	O	HO ₂	12.1	H	HO ₂	1.8	N ₂ O	NO	0.0420
		CH ₃	S-CH ₂	0.0	HO ₂	H ₂ O	4.2	HO ₂	H ₂	0.9	N	NH	0.0357

^aInitial temperature $T = 800$ K.

both the forward and reverse reaction rates are taken into account in the current work. Equation 1 has been modified as eq 3

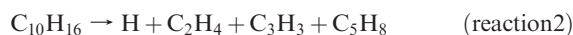
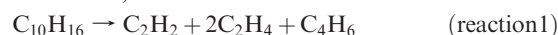
$$\dot{A}_{ijk}(t) = (|q_{i,\text{fwd}}(t)| + |q_{i,\text{rev}}(t)|) \frac{n_{A,j} n_{A,k}}{N_{A,i}} \quad (3)$$

where $q_{i,\text{fwd}}$ and $q_{i,\text{rev}}$ are the reaction rates of forward and reverse reactions, respectively.

For a complete characterization of the combustion process, one should perform multi-element flux analysis to account for transformations involving C, H, O, and N. Once calculated and sorted respectively, a user-selected cutoff is applied to the corresponding flux lists. Species above the cutoff correspond to larger fluxes and are retained in the reduced mechanism. Meanwhile, species below the cutoff are of trivial activity and are excluded from the current reduced mechanism. Note here that fluxes for each element are calculated and cut separately. The union set of reduced species sets for each element defines the reduced mechanism. This is due to the fact that different elements might have different flux values. If all element fluxes are sorted together, C, H, and O element fluxes will be much larger than the N flux. Thus, species with C, H, and O fluxes will be given higher ranks, while N-bearing species are always excluded from the reduced mechanism. To account for this variance, fluxes based on different elements are sorted and considered separately. While the element flux indicators provided by flux analysis describe the transition between two species, they also illustrate important connections between fuels and final products. These flux indicators can be used to identify the key pathways present in a detailed kinetic mechanism with minimum computational effort. By monitoring flux pointers in a dynamic mode, different stages of the system evolution can be captured.

To better illustrate the flux analysis methodology, we consider the stoichiometric JP-10/air oxidation and NO_x formation in a plug-flow reactor (PFR) model with an initial temperature of 800 K. First, flux analysis is performed for elements C, O, H, and N of JP-10 combustion in PFR to show the transition of different elements in the system. Element flux pointers at different stages are listed in Table 1. Because of the limitation of space, only the

first 10 source–sink pairs out of hundreds of pairs are shown. At the initial stage of combustion ($T = 805$ K), JP-10 decomposition is the dominant part of the entire pathway. As shown in Table 1, carbon flux analysis captures active hydrocarbon species at the initial stage, most of which are from JP-10 decomposition reactions (reactions 1–3).



It should be pointed out that these reactions are not elementary reactions. Instead, some overall approximations were employed to combine a series of elementary reaction steps. This is due to the fact that JP-10 is too large of a molecule for a complete detailed chemical mechanism of its decomposition and combustion to be developed, which was indicated by the authors of the mechanism.² Hydrogen flux captures active H-bearing radicals and species such as H, HO₂, and hydrocarbons. Oxygen flux identifies active O-bearing radicals and species such as O₂, OH, and O. Most of these active species captured by hydrogen and oxygen flux are involved in facilitated JP-10 decomposition. Active species of NO_x formation can be identified through the associated N fluxes, although flux values are much smaller than carbon, hydrogen, and oxygen. As the system temperature increases to 1500 K, oxidation of small hydrocarbons, such as C₂H₂ and C₂H₄, become dominant. For the NO_x formation network, similar source–sink pairs have been identified with flux magnitudes increased by a factor of 10. When the system temperature further increases to 2700 K, the combustion process reaches the final stage, where reactions from intermediates to final products CO₂ and H₂O become dominant. Meanwhile, a high temperature significantly promotes NO_x formation; flux values are increased by a factor of 100 compared to the initial stage. NO, NO₂, and N₂O are formed with the highest rates throughout the combustion process. As shown in Table 1, a small portion of source–sink

pairs can capture most of the element transformation in the system. This is due to the fact that, at a certain phase of a combustion process, only part of the overall pathway is active, while the rest shows little or no activity. Thus, as the combustion process evolves, different components of the pathway become active.

The proposed reduction scheme is able to capture the reactive propensity of the system by employing multi-element flux analysis. However, when the scheme is applied to hydrocarbon oxidation mechanisms with soot formation, soot species and precursors, also analyzed through C fluxes, are usually given low ranks because of their small flux values compared to the fuel oxidation network. It should be pointed out that in our illustration using JP-10/NO_x, although the NO_x formation network also has a much smaller flux compared to JP-10 oxidation, the reactive propensity of N-bearing species can be captured by nitrogen element flux. However, a soot formation network usually consists of PAH evolution and their aggregation to soot, which involves the same elements (C, H, and O) as fuel oxidation. Thus, there is no unique element that can capture soot formation separately. To incorporate soot formation kinetics in mechanism reduction, a kinetic network separation algorithm should be incorporated in the on-the-fly scheme. The objective of this procedure is to separate the soot formation network from the fuel oxidation network. The species in the two separate networks are analyzed and reduced independently on the basis of element flux. Then, the two reduced species sets are combined, and reactions only involving species in the combined set are kept in the reduced mechanisms. Identifying the reaction set based on the combined species set ensures that interactions between different networks will be included in the reduced mechanism.

For the separation of two kinetic networks, we explore concepts similar to graph partitioning, i.e., the process of dividing a graph into pieces, algorithms. There are three major categories of graph partitioning algorithms: (a) spectral methods,^{31,32} which seek a partition that maximizes the intracommunity connections while minimizing intercommunity connections based on an adjacency matrix, (b) recursive partitioning,³³ which starts the partitioning procedure by dividing the original graph into a certain number of subgraphs and further divides them if desired, and (c) local agglomeration,^{34,35} in which subgraphs are agglomerated on the basis of selected nodes until certain criteria are satisfied. The subgraphs identified by spectral methods have the maximum intracommunity connectivity; however, the subgraphs might include both soot species and fuel oxidation species. Therefore, the method is unable to effectively separate the soot formation from the fuel oxidation network. Recursive partitioning methods can provide a partition of the original graph with a user-defined number of subgraphs. However, when implemented in our work to separate different reaction networks, recursive partitioning also fails to discriminate soot formation species and fuel oxidation species. The local agglomeration method starts from specific nodes and groups neighboring nodes based on the strength of connections. It is able to separate different subnetworks by initializing agglomeration from species that are exclusively involved in each subnetwork, which well serves the purpose of network separation in this work. In the present study, because both the soot formation and fuel oxidation originate from JP-10,

we employ reverse agglomeration, which starts from the final products of the two subnetworks. PAHs and CO₂ are selected to initialize the soot formation and fuel oxidation agglomeration, respectively. The algorithm takes PAHs and CO₂ as tree root and searches backward the entire reaction network to identify their source species. Then, these source species are considered as sink species in the next iteration. The algorithm proceeds until no new sources can be identified. After completion of the searching part, soot formation and JP-10 oxidation subnetworks that terminate at PAHs and CO₂, respectively, are separated. Figure 1 shows the soot formation (red edges) and JP-10 oxidation (black edges) subnetworks. For simplicity, only a part of the graph is shown. It can be observed from the flux graph that overlap exists between the two subnetworks (blue edges). The overlapping part is assigned to the fuel oxidation network because source–sink pairs in this part have comparable flux magnitudes to the fuel oxidation network, while being much greater than the corresponding components of the soot formation network. For the JP-10/soot mechanism used in the present work, the entire flux graph constitutes 748 edges, 58 of which are located in the soot formation network and 690 are included in JP-10 oxidation network. Given the two separate subnetworks, flux analysis is employed on each subnetwork to identify active soot formation and JP-10 oxidation species. Two reduced species sets are then combined, and reactions involving these active species are identified to form the kinetic mechanism for a given time step.

The mechanism reduction scheme based on flux analysis provides an efficient method to couple detailed chemistry with CFD calculation. The on-the-fly reduction scheme, as the name suggests, involves the dynamic identification of reduced mechanisms during the simulation. In practice, element flux analysis is carried out at every time step of the CFD calculation, and a reduced mechanism is developed on the basis of active species and reactions identified through flux analysis. The reduced mechanism defines the chemistry of the current time step, and species in the reduced mechanism are integrated. However, all of the species are transported, and all species concentrations are stored in the flow calculation, so that when a different set of active species are identified at other time steps, the required species information can be retrieved to initialize the kinetic calculation for the given time step.

Characterization of JP-10 Combustion and Pollutant Formation

The proposed element flux analysis is demonstrated using a JP-10/NO_x chemical mechanism consisting of 56 species and 260 reactions.² Predicted results with the on-the-fly reduction method are compared to simulations with the detailed mechanism and the experimental data of Mikolaitis et al.³⁶ in Figure 2. The on-the-fly reduced representation reproduces the ignition delay of JP-10 with good agreement compared to detailed simulations. Figure 3 compares the CPU time for simulations using the complete mechanism and the on-the-fly scheme with an initial temperature of 1500 K. The CPU of the PFR simulation can be divided into three parts: flow calculation, chemistry calculation, and flux analysis overhead. The CPU time of each part is shown in Figure 3. Because all of the species are transported in the flow calculation, the CPU time on flow calculation of two schemes is similar. However, the on-the-fly scheme reduces the mechanism size, which saves CPU time on chemistry calculation by a factor of 4 in PFR simulation. As shown in Figure 3, the overhead introduced by flux analysis is 24.8 s, which accounts for 8.6% of the total CPU time.

(31) Karypis, G.; Kumar, V. A fast and high quality multilevel scheme for partitioning irregular graphs. *SIAM J. Sci. Comput.* **1998**, *20* (1), 359–392.

(32) Karypis, G.; Kumar, V. Multilevel *k*-way partitioning scheme for irregular graphs. *J. Parallel Distrib. Comput.* **1998**, *48* (1), 96–129.

(33) Hsieh, S. H.; Paulino, G. H.; Abel, J. F. Recursive spectral algorithms for automatic domain partitioning in parallel finite-element analysis. *Comput. Methods Appl. Mech. Eng.* **1995**, *121* (1–4), 137–162.

(34) Prasad, L.; Skourikhine, A. N. Vectorized image segmentation via trixel agglomeration. Proceedings of Graph-Based Representations in Pattern Recognition, 2005; Vol. 3434, pp 12–22.

(35) Prasad, L.; Skourikhine, A. N. Vectorized image segmentation via trixel agglomeration. *Pattern Recognit.* **2006**, *39* (4), 501–514.

(36) Mikolaitis, D. W.; Segal, C.; Chandy, A. Ignition delay for jet propellant 10/air and jet propellant 10/high-energy density fuel/air mixtures. *J. Propul. Power* **2003**, *19* (4), 601–606.

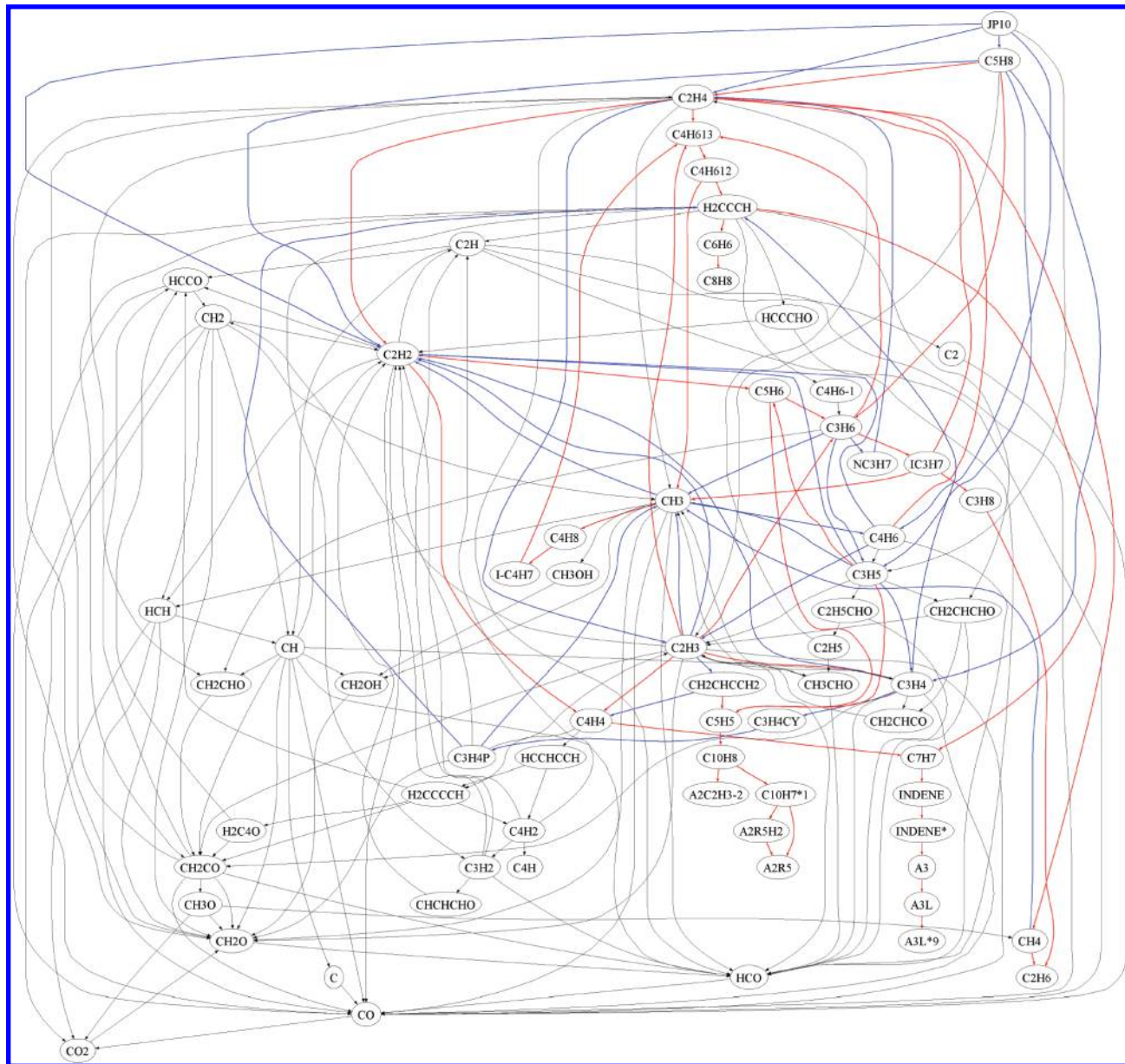


Figure 1. Flux graph of JP-10 oxidation with PAH formation. Red edges, PAH formation network; black edges, JP-10 oxidation network; blue edges, overlap of two networks.

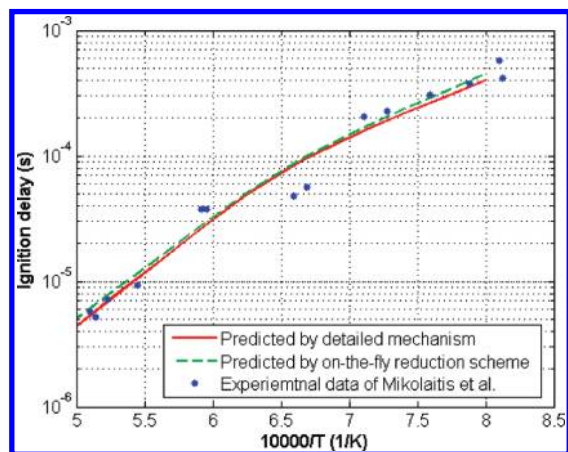


Figure 2. Ignition delay time of stoichiometric JP-10/air combustion predicted by simulations using a detailed mechanism and an on-the-fly reduction scheme compared to experimental data.

To characterize JP-10 combustion with NO_x formation, the on-the-fly scheme is integrated with the KIVA-3V CFD code.³⁷ A two-dimensional numerical mesh (Figure 4) with moving boundaries was employed to simulate a homogeneous charge compression ignition (HCCI) engine. CHEMKIN³⁸ is used for solving the chemistry during the engine simulation. During the calculation, flux analysis is performed at each grid cell at every time step. A flowchart summarizing the integrated framework is provided in Figure 5. The detailed mechanism includes n_s species. The flux analysis identifies a reduced species set containing

(37) Amsden, A. A. KIVA-3V: A block-structured KIVA program for engines with vertical or canted valves. Los Alamos National Laboratory Report LA-13313-MS, Los Alamos National Laboratory, Los Alamos, NM, 1997.

(38) Kee, R. J.; Rupley, F. M.; Meeks, E.; Miller, J. A. CHEMKIN-III: A FORTRAN chemical kinetics package for the analysis of gas-phase chemical and plasma kinetics, SAND-96-8216, Sandia National Laboratories, Livermore, CA, 1996.

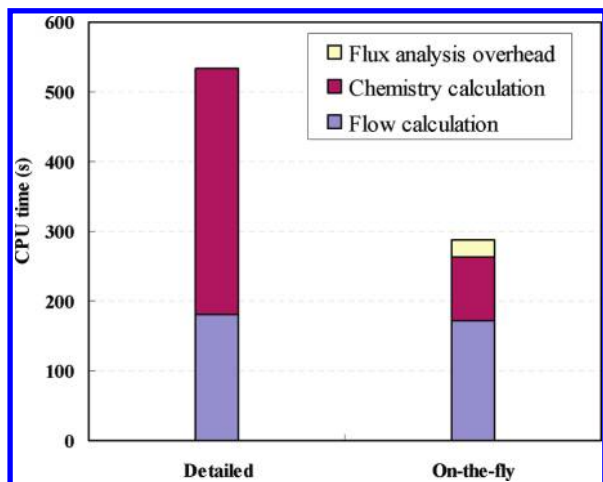


Figure 3. CPU time of stoichiometric JP-10/air combustion simulation in the PFR model.

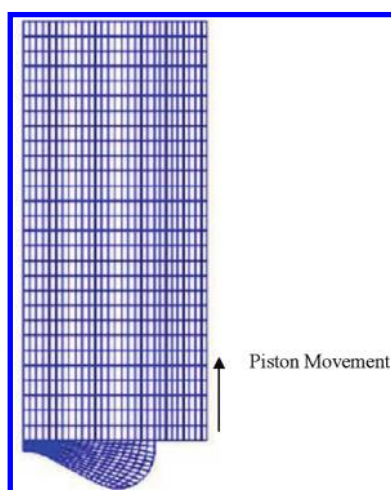


Figure 4. Two-dimensional numerical mesh of KIVA simulation.

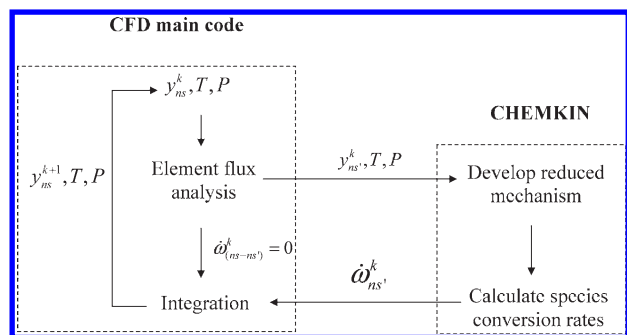


Figure 5. Integration of CHEMKIN application with CFD code.

$ns' \leq ns$ species. The concentration of these ns' species $y_{ns'}^k$ along with the temperature and pressure are passed to CHEMKIN, where a reduced mechanism is generated and species conversion rates $\dot{\omega}_{ns'}^k$ are calculated. Meanwhile, the $ns - ns'$ species that are not included in the reduced mechanism are considered as dormant; i.e., chemical conversion rates $\dot{\omega}_{(ns-ns')}^k$ are set to be zero, and their concentrations are kept unchanged at the current time step. On the basis of the species conversion rates, all species concentrations are integrated and temperature and

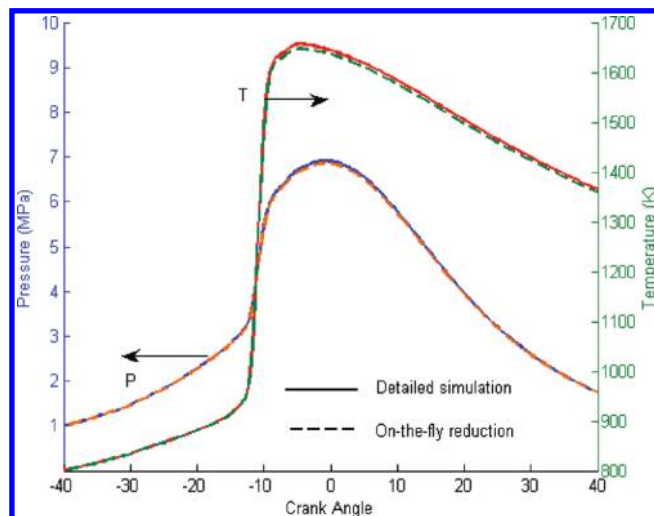


Figure 6. Temperature and pressure profiles of stoichiometric JP-10/air oxidation with NO_x formation in KIVA simulation. Initial conditions: $T = 800$ K and $P = 1$ MPa.

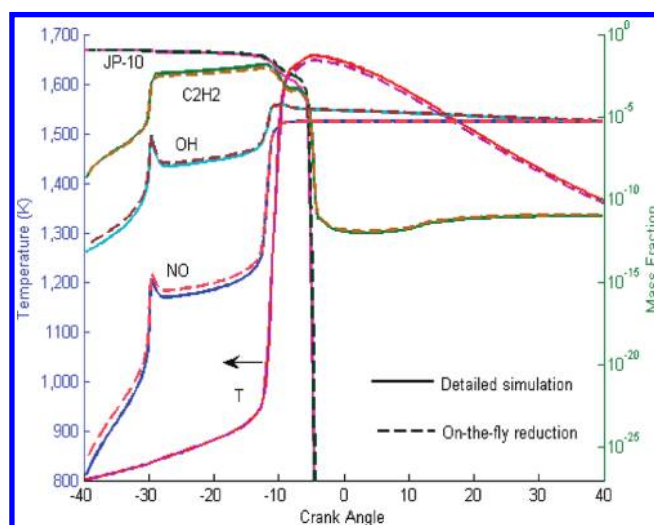


Figure 7. Selected species concentration profiles of stoichiometric JP-10/air oxidation with NO_x formation in KIVA simulation. Initial conditions: $T = 800$ K and $P = 1$ MPa.

pressure changes are evaluated in the main code. The model simulates combustion in a HCCI engine from crank angle -40° to 40° after top dead center (ATDC). Temperature and pressure profiles predicted by the detailed simulation and on-the-fly reduction scheme are illustrated in Figure 6. Both the ignition timing and the peak temperature and pressure can be reproduced by the on-the-fly scheme with good agreement. Selected species profiles of JP-10 oxidation and NO_x formation are compared in Figure 7. The initial stage of the combustion and the decomposition of JP-10 result in rapid accumulation of C_2H_2 , and the level of C_2H_2 is maintained during the ignition delay period. The OH radicals build up initially and then decrease for a short period early during the induction stage. As the level of JP-10 decreases further, the temperature and OH radical concentration increase rapidly and C_2H_2 is further oxidized. This delayed induction is due to the strong affinity of JP-10 for radicals. The existence of a high level of JP-10 in the system consumes

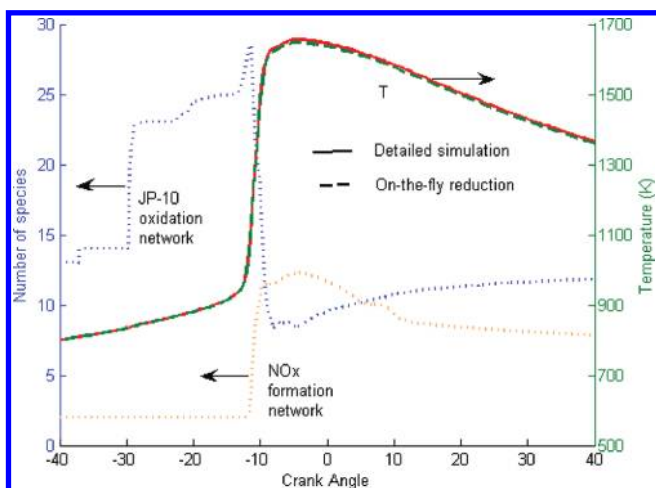
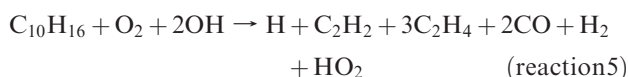
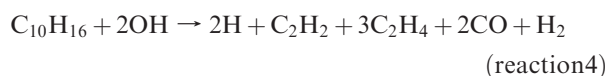


Figure 8. Mechanism size of stoichiometric JP-10/air oxidation with NO_x formation. Initial conditions: $T = 800$ K and $P = 1$ MPa.

most of the OH radical through overall reaction steps 4–6.²



These reactions result in the net consumption of OH radicals, which is the major source of induction delay in JP-10 combustion.² The NO_x formation in JP-10 combustion is highly correlated to the OH concentration. As shown in Figure 7, the NO concentration accumulates in the initial stage and decreases over a short period as OH is consumed by JP-10. When JP-10 drops to a low level and OH further increases, NO is formed rapidly and reaches its maximum value when the system ignites. The on-the-fly reduction scheme reproduces the detailed simulation results with excellent accuracy. Both the induction and ignition stages are well-characterized with the reduced representation.

The reduced mechanism sizes for JP-10 oxidation and NO_x formation are compared in Figure 8 in terms of species numbers. At the initial stages, the decomposition of JP-10 is the most significant part of the reaction network, thus small mechanisms were generated, including only JP-10 and its decomposition products. During the induction stage, the mechanism size of the JP-10 network grows because of the increased activity of JP-10 decomposition and radical pool buildup. When the system ignites, a large amount of radicals and intermediate species are generated, which results in an even larger JP-10 oxidation network. The size of JP-10 oxidation reaches its maximum level at the beginning of the ignition stage, at which point molecules and radicals have the highest activity. However, it can be observed in Figure 8 that the NO_x formation network evolves through a different pattern. The network grows after the system ignites. This is due to the fact that the oxidation of N_2 may occur only when the system temperature reaches a certain level. After ignition, a high system temperature expedites N_2 dissociation, which initiates NO_x formation. The network size evolution shown in

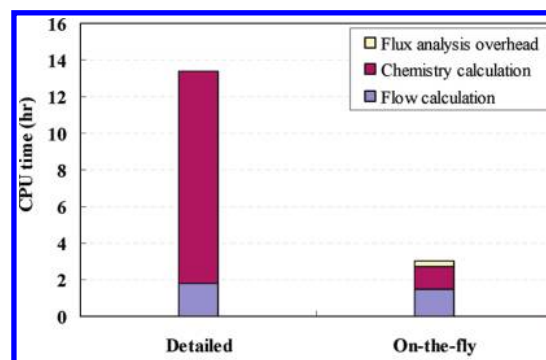


Figure 9. CPU time of stoichiometric JP-10/air combustion simulation with NO_x formation in KIVA using the detailed mechanism and on-the-fly reduction scheme. Initial conditions: $T = 800$ K and $P = 1$ MPa.

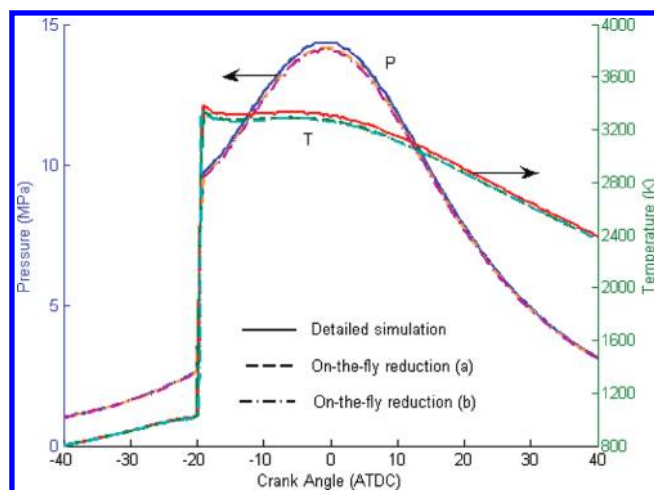


Figure 10. Temperature and pressure profiles of stoichiometric JP-10/air oxidation with soot formation in KIVA simulation: (a) soot formation separated from JP-10 oxidation and (b) soot formation not separated from JP-10 oxidation. Initial conditions: $T = 800$ K and $P = 1$ MPa.

Figure 8 indicates that NO_x formation lags fuel oxidation in the combustion process. The average mechanism size of the entire KIVA simulation is 21 species and 121 reactions compared to 56 species and 260 reactions for the complete mechanism. Figure 9 compares the CPU time of the detailed simulation and on-the-fly reduction scheme. The CPU time spent on chemistry calculation is reduced by a factor of 10, while the overhead introduced by flux analysis comprises 8.2% of the total CPU time.

To study soot formation in JP-10 combustion, the element flux analysis and on-the-fly scheme are applied on a JP-10/soot mechanism constitute of 161 species and 900 reactions, which is created by combining a JP-10 mechanism and a PAH formation mechanism. The JP-10 decomposition and oxidation kinetics is from the JP-10 oxidation mechanism,² and the kinetics of C2–C5 oxidation and PAH formation are described by the mechanism developed by Richter et al.³⁹ The tree-building search algorithm described in the previous section is employed to separate the soot formation subnetwork from the fuel oxidation network. The KIVA simulation is monitored from crank angle -40° to 40° for stoichiometric

(39) Richter, H.; Benish, T. G.; Ayala, F.; Howard, J. B. Kinetic modeling of the formation of polycyclic aromatic hydrocarbons. *Abstr. Pap. Am. Chem. Soc.* **2000**, *219*, U679–U679.

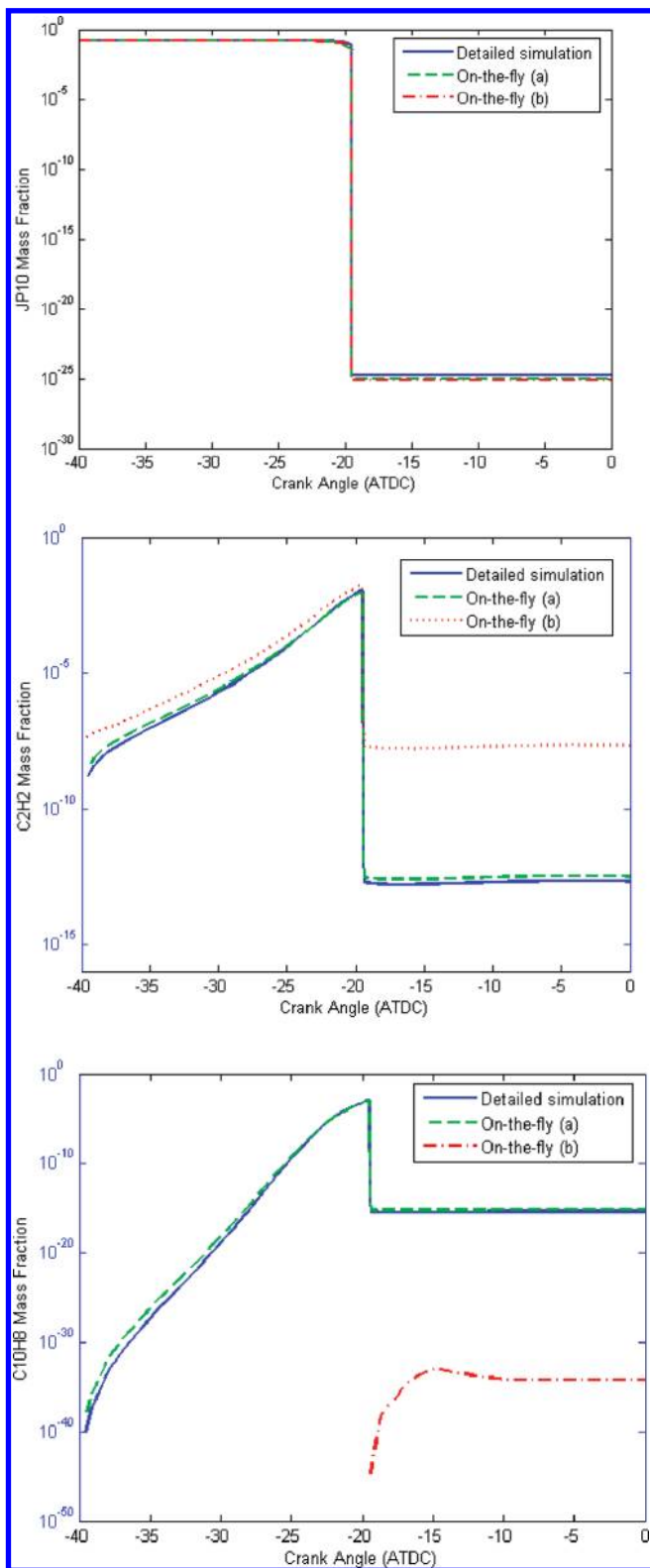


Figure 11. JP-10, C_2H_2 , and $C_{10}H_8$ species mass fraction profiles of stoichiometric JP-10/air oxidation with soot formation in KIVA simulation: (a) soot formation separated from JP-10 oxidation and (b) soot formation not separated from JP-10 oxidation. Initial conditions: $T = 800$ K and $P = 1$ MPa.

JP-10/ O_2 /Ar combustion with an initial temperature of 800 K and pressure of 1 MPa. Figure 10 compares the temperature and pressure profiles of the detailed simulation, the on-the-fly reduction on two separate flux graphs (scheme a), and the

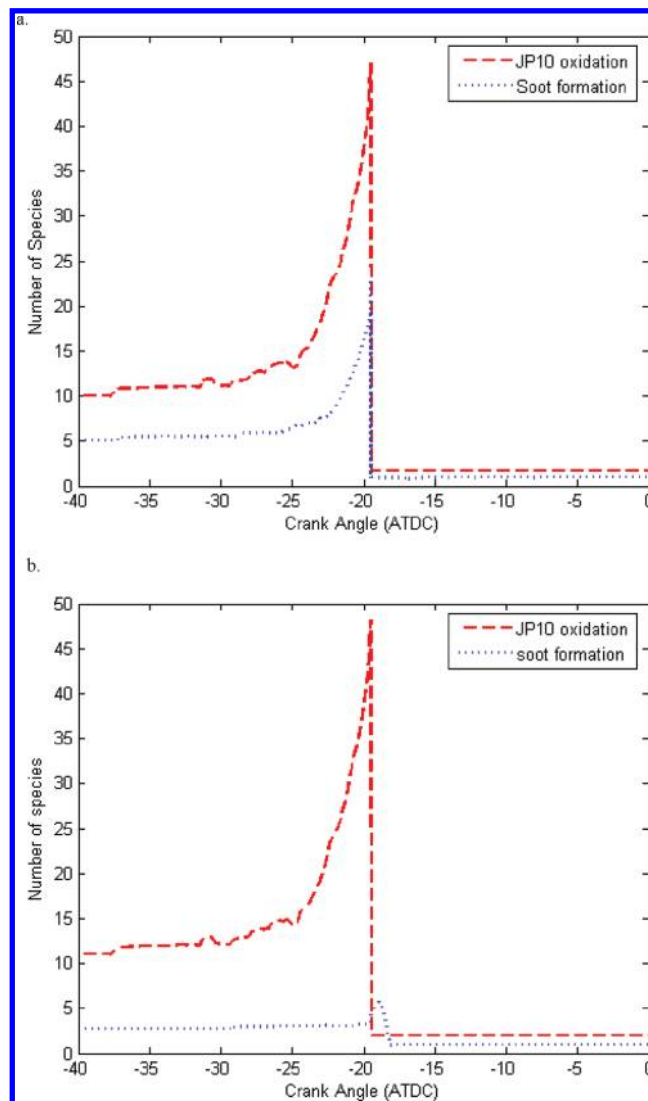


Figure 12. Mechanism size of stoichiometric JP-10/air oxidation and soot formation: (a) soot formation network separated from JP-10 oxidation and (b) soot formation not separated from JP-10 oxidation. Initial conditions: $T = 800$ K and $P = 1$ MPa.

on-the-fly scheme without separation of soot formation from JP-10 oxidation (scheme b). It can be observed in Figure 10 that applying different analysis schemes for the soot network does not significantly affect the temperature and pressure profiles. This is due to the fact that soot formation has very small flux and, thus, makes only a very small contribution to thermo-physical properties of the system, such as temperature and pressure. However, the effect of properly accounting for soot formation is significant when considering the overall combustion process. Figure 11 compares the profiles of JP-10, C_2H_2 , and $C_{10}H_8$ concentrations of schemes a and b. $C_{10}H_8$ is one of the major PAHs formed in hydrocarbon combustion, and C_2H_2 plays an important role in PAH formation.⁸ Thus, these two species are characteristic of the soot formation network and are chosen to compare different analysis schemes in this work. It can be seen in Figure 11 that JP-10 concentrations are not affected too much by two different schemes because soot formation consumes very small portions of hydrocarbons in the system. On the other hand, C_2H_2 and $C_{10}H_8$ exhibit distinct profiles in the two different schemes. In scheme a, where the soot network is sepa-

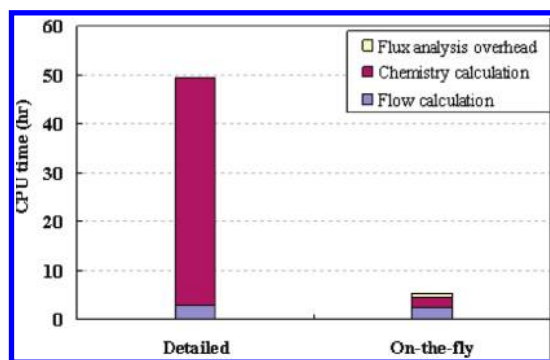


Figure 13. CPU time of stoichiometric JP-10/air combustion simulation with soot formation in KIVA using the detailed mechanism and on-the-fly reduction scheme. Initial conditions: $T = 800$ K and $P = 1$ MPa.

rated from JP-10 oxidation, C_2H_2 and $C_{10}H_8$ are predicted accurately compared to the detailed simulation, while in scheme b, where reduction is performed on the entire network, soot formation networks are not included in the reduced mechanisms because of their small flux. Therefore, the mass fraction of C_2H_2 after ignition is much higher in scheme b because soot formation is not included and C_2H_2 is less consumed. Similarly, in scheme b, $C_{10}H_8$ is not well-predicted because only after the ignition when the flux of JP-10 oxidation network drops to a low level, can the soot formation network have a higher rank and be considered in the reduced mechanisms. Thus, before ignition, no $C_{10}H_8$ is produced, and after ignition, $C_{10}H_8$ starts to accumulate but is still much lower than the detailed simulation results. The effect of network separation is further demonstrated in Figure 12, where the reduced network sizes of two schemes in terms of species numbers are compared. As shown in Figure 12, when soot formation is not separated from JP-10 oxidation, very few species in the soot formation network are included in the reduced mechanisms before ignition. After the ignition, when the flux of JP-10 oxidation drops to very low levels, more species are included in the mechanism. On the other hand, when soot formation is separated from JP-10 oxidation, the number of species used to describe soot formation has a similar pattern with JP-10 oxidation. In the induction stage, the number of species that soot kinetics increases, and after ignition, the mechanism size drops to a low level. This pattern agrees with the $C_{10}H_8$ concentration profile, as shown in Figure 11. The average size of the reduced mechanisms is 26 species and 192 reactions compared to 191 species and 900 reactions for the complete mechanism. CPU times of the detailed simulation and on-the-fly scheme are compared in Figure 13. The on-the-fly reduction scheme reduces CPU time on chemistry calculation by a factor of 25, and the overhead introduced by flux analysis of two networks comprises 11.6% of the total CPU time.

Concluding Remarks

The element flux analysis enables the detailed characterization of fuel oxidation pathways and pollutant formation mechanisms. The on-the-fly kinetic reduction scheme based on element flux analysis provides an efficient way to incorporate detailed kinetic mechanisms in CFD calculations. A multi-element flux analysis has been proposed to address transitions and transformations of different elements in the system. Element fluxes of carbon, oxygen, and hydrogen are analyzed separately to capture fuel oxidation and radical transitions. In addition, nitrogen flux is used to describe NO_x formation in the system. However, for soot formation, there is no unique element that can capture the network. To include soot formation in kinetic reduction, a network separation algorithm has been complemented to the on-the-fly reduction scheme. Soot formation and fuel oxidation networks are identified by searching from PAHs and CO_2 , respectively. The two networks are reduced separately, and two reduced mechanisms are combined to define local chemistry. In the present work, a chemical mechanism of JP-10 oxidation along with NO_x and soot formation is investigated using the proposed method. Because of the large size of the JP-10 “molecule”, the detailed description of JP-10 oxidation is difficult. Therefore, the mechanism used in this paper employed overall approximations in JP-10 non-oxidative pyrolytic decomposition and oxidative pyrolysis steps to obtain a short mechanism that arrives as quickly as possible at C_1 – C_3 chemistry, for which a detailed mechanism has been developed.^{2,40,41} The selection of this mechanism in this work represents the first attempt to perform the simulation of JP-10 combustion in CFD using complex chemical mechanisms. However, the incorporation of a complete JP-10 chemical mechanism would be worthwhile in our future work.

Ignition delays of JP-10 are predicted in a PFR model and engine simulations using the KIVA-3V code, respectively. The numerical results show excellent agreement with experimental data obtained for the literature, and CPU time is reduced dramatically compared to calculations using the full mechanism. It is demonstrated that, by implementing the multi-element flux analysis and network separation algorithm, the proposed on-the-fly scheme is able to incorporate both fuel combustion and pollutant formation in CFD calculation, which facilitates the numerical study of fuel combustion.

Acknowledgment. The authors gratefully acknowledge financial support from ExxonMobil R&E Co., National Science Foundation (NSF) CBET Grant 0730582, and Office of Naval Research (ONR) Contract N00014-06-10835.

(40) Varatharajan, B.; Williams, F. A. Ethylene ignition and detonation chemistry. Part 1: Detailed modeling and experimental comparison. *J. Propul. Power* **2002**, *18* (2), 344–351.

(41) Varatharajan, B.; Williams, F. A. Ethylene ignition and detonation chemistry. Part 2: Ignition histories and reduced mechanisms. *J. Propul. Power* **2002**, *18* (2), 352–362.